

# Design, Synthesis, and Characterization of Globular Orphan Nuclear Receptor Regulator with Biological Activity in Soft Tissue Sarcoma

Mao Ye,<sup>†,◇</sup> Santosh K. Misra,<sup>†,◇,ID</sup> Arun K. De,<sup>‡,§,◇</sup> Fatemeh Ostadhossein,<sup>†</sup> Kuldeep Singh,<sup>||</sup> Laurie Rund,<sup>‡,§,||</sup> Lawrence Schook,<sup>‡,§,||</sup> and Dipanjan Pan<sup>\*,†,‡,§,||,∇,○,ID</sup>

<sup>†</sup>Department of Bioengineering, University of Illinois at Urbana–Champaign, Urbana, Illinois 61801, United States

<sup>‡</sup>Department of Animal Sciences, University of Illinois at Urbana–Champaign, Urbana, Illinois 61801, United States

<sup>§</sup>Agricultural Animal Care and Use Program, University of Illinois at Urbana–Champaign, Urbana, Illinois 61801, United States

<sup>||</sup>Veterinary Diagnostic Laboratory, University of Illinois at Urbana–Champaign, Urbana, Illinois 61801, United States

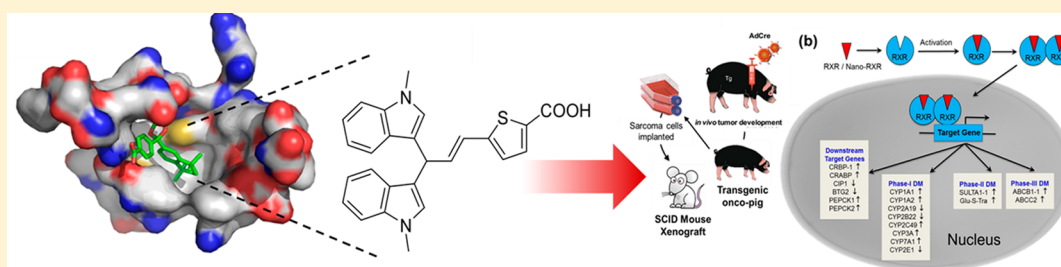
<sup>∇</sup>Beckman Institute of Advanced Science and Technology, University of Illinois at Urbana–Champaign, Urbana, Illinois 61801, United States

<sup>○</sup>Mills Breast Cancer Institute, Carle Foundation Hospital, 502 N. Busey, Urbana, Illinois 61801, United States

<sup>∇</sup>Department of Materials Science and Engineering, University of Illinois at Urbana–Champaign, Urbana, Illinois 61801, United States

<sup>○</sup>Carle-Illinois College of Medicine, Urbana, Illinois 61801, United States

## Supporting Information



**ABSTRACT:** Sarcomas are rare and heterogeneous cancer variants of mesenchymal origin. Their genetic heterogeneity coupled with uncertain histogenesis makes them difficult to treat and results in poor prognosis. In this work, we show that structure-based drug discovery involving computational modeling can be used to identify a new retinoid X receptor (RXR) agonist ligand with a bis(indolyl)methane scaffold. This agent co-self-assembles with an amphiphilic diblock copolymer resulting in nanoparticles (Nano-RXR) with excellent kinetic stability, which were evaluated for efficacy and safety in transformed sarcoma cells, 63-3 Cre and 141-10 Cre of pig origin, and in rodent xenograft models. Responses at gene and protein levels established the treatment approach as a highly effective RXR agonist across cell, rodent, and “Oncopig” models. Interestingly, Nano-RXR was not only able to modulate metabolic and transporter genes related to orphan nuclear receptors but also played a major role in modulating programmed cell death in sarcomas developed in Oncopigs.

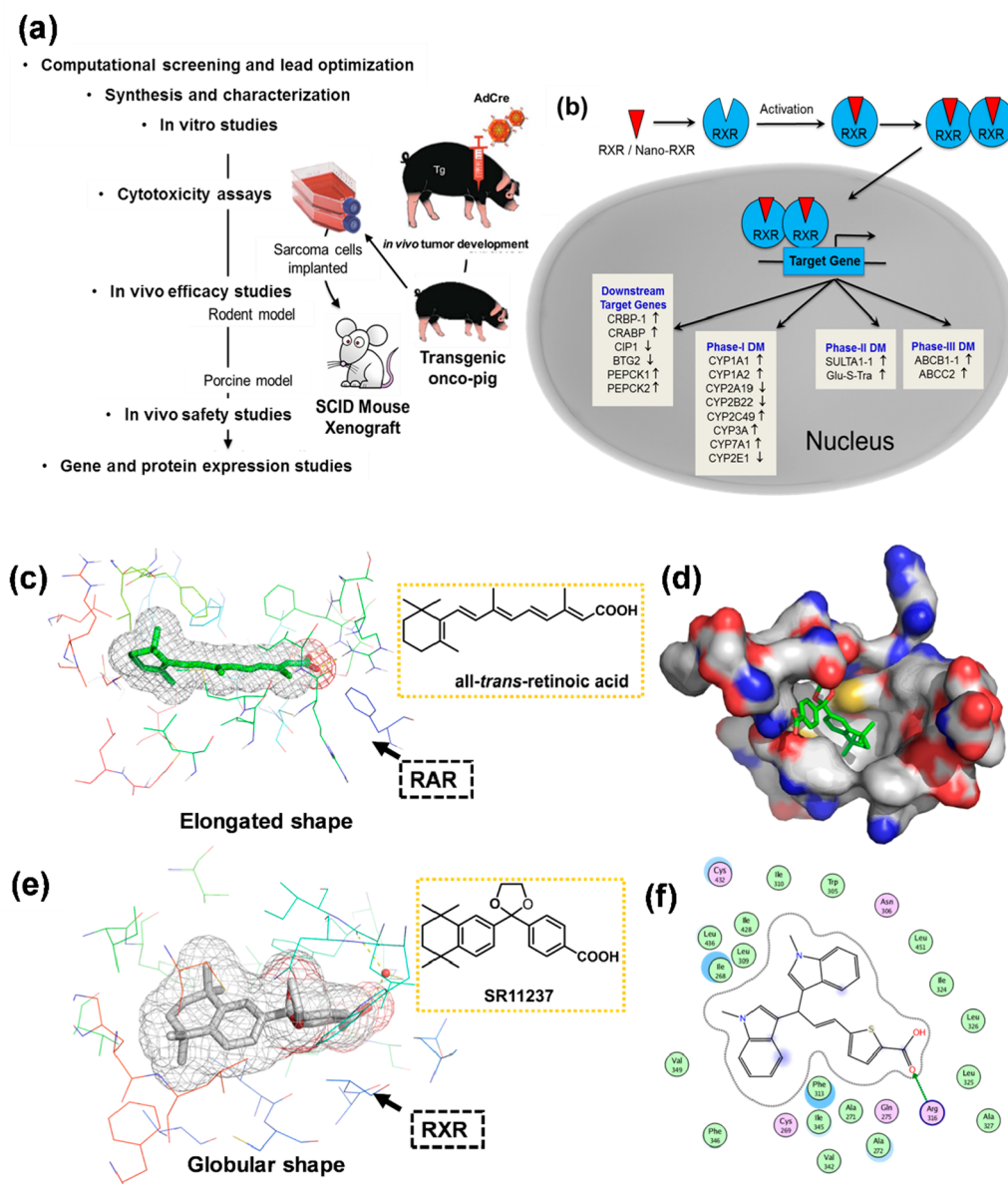
## INTRODUCTION

Sarcomas generally require surgical resection and radiation as standard care in high-risk patients.<sup>1</sup> Despite aggressive intervention, nearly 50% of patients suffer from recurrent disease leading to death. Some sarcomas are sensitive to chemotherapy with greatly improved treatment results. One such group of sarcomas where chemotherapy increased survival from 20% to 70% is localized osteosarcoma.<sup>2</sup> The effectiveness of immunotherapy in the metastatic soft tissue sarcomas is also being evaluated in clinical trials.<sup>3</sup> Despite this promise, the last two decades have seen a plateau in this progress, and chemotherapy has not altered the poor patient outcome associated with metastatic disease. There is no universally accepted neoadjuvant therapy standard of care.<sup>2–11</sup> Though several clinical studies indicated that neoadjuvant therapy with

doxorubicin (DOX) and ifosfamide (AIM), epirubicin and ifosfamide, or doxorubicin, ifosfamide, and dacarbazine (MAID) with or without radiation therapy improved survival in high-risk patients, none of the phase III randomized trials offered unequivocal positive results for neoadjuvant therapy in soft tissue sarcomas, making these chemotherapy trials heterogeneous and outcomes conflicting. Furthermore, the response of older patients toward current medication is constrained by factors such as the associated toxicity. This plus other comorbidities arising from chemotherapy warrants the pursuit of novel therapies for this aggressive disease. Future progress may include the discovery of new cytotoxic chemotherapeutics

Received: September 5, 2018

Published: October 30, 2018

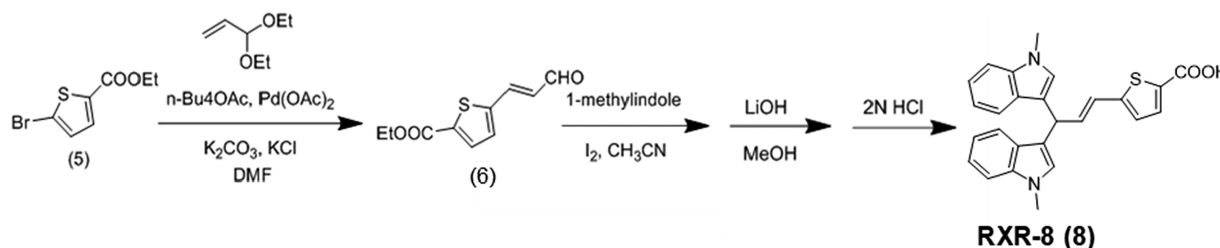


**Figure 1.** Outline of planned research to evaluate in vitro and in vivo efficiencies. (a) Progression of computational, chemical, and biological experiments and (b) summary of gene regulations expected from newly designed RXR agonist in vivo. In-silico studies to identify RXR agonist through lead optimization. (c) Elongated shape of RAR and (d) globular shape of RXR structures; (e) Molcad Surfaces of IMVC, RXR agonist conformation crystal structure and (f) ligand interaction pictures of docking structures of compound 8.

and development of targeted therapies with controlled release pathways.<sup>12–23</sup> An evaluation of their role in metabolic and transport gene regulation and their effective induction of genes in the programmed cell death cascade would enhance their utility in future clinical trials.

Retinoid X receptor (RXR) is a master regulator of multiple biological processes due to the formation of heterodimers with other nuclear receptors. RXR ligands or rexinoids are found to activate permissive heterodimers, or subordinate to the partner ligand in nonpermissive heterodimers to act cooperatively or synergistically. The negative cooperativity in RXR–thyroid hormone receptor (TR) heterodimers has been found to be due to the allosteric repression of TR by rexinoids. In general, agonists, partial agonists, and antagonists exert different roles in the heterodimers by strengthening or disrupting the interaction surface with co-regulators. The activity of the partial agonists and antagonists could depend on the cellular context and the

nature of co-regulators. Thus use of partial antagonists or agonists to overcome undesired effects of rexinoids is a promising new avenue for therapy. For instance, bexarotene and alitretinoin (9-*cis*-retinoic acid) are in the clinic for topical and systemic treatment of cutaneous T cell lymphoma (CTCL) and for the topical treatment of Kaposi's sarcoma and systemic treatment of refractory chronic hand eczema, respectively. RXR modulators also hold therapeutic potential for the treatment of diabetes and obesity, as well as atherosclerosis, other cardiovascular indications, and inflammatory diseases, but important secondary effects have been noted in rodent models, among them hypertriglyceridemia, suppression of the thyroid hormone axis, and induction of hepatomegaly. Recently described therapeutic options for rexinoids in cancer and neurodegeneration have opened exciting avenues for drug design and discovery of this important family of modulators. Nuclear hormone receptors, including RXR and peroxisome

Scheme 1. Chemical Synthesis and Characterization of Compound 8<sup>a</sup>

<sup>a</sup>For the designed RXR-agonist **8**, aryl bromide **5** with acrolein diethyl acetal in the presence of *n*-Bu<sub>4</sub>OAc, K<sub>2</sub>CO<sub>3</sub>, KCl, and DMF catalyzed by Pd(OAc)<sub>2</sub> afforded cinnamaldehyde **6** in 73% yield. Bis(indolyl)methane compound **7** was obtained in 81% yield from **6** and 1-methylindole catalyzed by molecular iodine in CH<sub>3</sub>CN at room temperature. Hydrolysis of **7** with LiOH·H<sub>2</sub>O in methanol and acidification afforded the final product **8** in 91% yield.

proliferator-activated receptor (PPAR), represent therapeutic targets in sarcoma. RXRs have been considered as “auxiliary” receptors that enhance DNA binding of retinoic acid receptor (RAR) and other nuclear hormone receptors, including PPAR $\gamma$ . More recent studies, however, showed that selective activation of RXR could lead to transcriptional activation, apoptosis, and redifferentiation of embryonal carcinoma cells and that the effects of RAR and RXR selective agents in combination had synergistic effects. PPAR $\gamma$  receptors have been studied in primary human tissues with positive immunostaining for PPAR $\gamma$  in 14/14 nevi, 10/11 primary sarcoma lesions, and 6/8 sarcoma metastases. Similarly, high in vitro and in vivo activities were reported on PPAR $\gamma$  expressing sarcoma cells with significant reduction in cell proliferation.

Toward this aim, we provide an “in silico to in vivo” approach to identify and synthesize an RXR agonist. Furthermore, we developed it as a nanotherapy<sup>24–29</sup> treatment for “soft” tissue sarcoma, which can provide potent and controlled delivery of the newly discovered retinoid X-receptor (RXR)-selective agonist (Figure 1a). RXR-selective agonists with new chemistry and approach were identified through structure-based drug discovery and computational modeling to transcriptionally activate the orphan nuclear receptor target.<sup>30–40</sup> The delivery of the potent agent has been accomplished by a micellar polymeric nanoparticle. The structurally new scaffold-based RXR selective agonist is different from either bexarotene or alitretinoin (9-*cis*-retinoic acid)-based structures, basic frames for most reported RXR ligands. Our results demonstrated significant efficacy in vitro. In order to realize the translational supremacy of the work, the agents were studied simultaneously in a rodent and a transgenic swine model (Oncopigs) of soft tissue sarcoma.<sup>41–43</sup> The Oncopig provides an inducible and reproducible tumor model in a large animal that is comparable to humans in both size and physiology and is being used for development, validation, safety, and efficacy assessment of the RXR agent intended for human translation. Studies with rodent and Oncopig models elucidate mechanistic insights into the modulations of RXR $\alpha$  PPAR transcriptional activation and downstream target genes along with genes involved in phase-I, phase-II, and phase-III metabolism and transport regulation in treated and control tumor tissues (Figure 1b).

## RESULTS AND DISCUSSION

**Structure-Based Design, Lead Optimization, and Synthesis of RXR Agonists.** Due to the high similarity of RXR and RAR structures, the selectivity of RXR over RAR is the key for the design of RXR ligands. Computationally, the RAR

structure has an elongated shape (Figure 1c), whereas RXR is globular and “L” shaped (Figure 1e). The interactions between the hinge region of the ligand and residues C432 and I268 are important for RXR selectivity. The Molcad surface picture in Figure 1d shows a relatively large L-shaped binding cavity in RXR structure, with hydrogen bond and ion–salt interactions on one end and a hydrophobic interaction on the other end. The thiol group from C432 forms a hydrogen bond with the oxygen in the bridge of a known RXR modulator SR11237 (alternatively called BMS649), making an important contribution to maintain the “L” shape of the structure. This suggests that an RXR agonist with an indole as the hydrophobic ring and another indole as the bridge substituent could be successfully derived from the bis(indolyl)methane moiety via structure-based lead optimization approach. Through computational modeling (Flow charts S1 and S2), we predicted that compound **8** could be a proper RXR ligand due to the ion–salt and hydrogen bond interactions with R316 and A327, and the hydrophobic interactions with I345, F346, and V349. Moreover, the N atom in the 1-methylindole of compound **8** forms a hydrogen bond with C432, and the 1-methyl group forms hydrophobic interactions with N306 and W305. Figure 1f shows the ligand interactions of compound **8** with residues in the 1MVC (crystal structure of the human RXR $\alpha$  ligand binding domain bound to the synthetic agonist compound BMS 649 and a coactivator peptide) structure. Based on these observations, compound **8** was synthesized as a structurally optimized RXR ligand. Our lead candidate is one of the first RXR agonists with an indole as the hydrophobic ring and another indole as the bridge substituent. Increasing the length of the bridge by a double bond makes stronger hydrogen bonds of the carboxylic acid with residues in the target. In addition, we anticipate that N-methylation makes stronger hydrophobic interactions. The flexible bridge between the hydrophobic end and the COOH end will make the compound more RXR selective.

For the synthesis of RXR-agonist **8** (RXR-8), aryl bromide **5** with acrolein diethyl acetal in the presence of *n*-Bu<sub>4</sub>OAc, K<sub>2</sub>CO<sub>3</sub>, KCl, and DMF catalyzed by Pd(OAc)<sub>2</sub> afforded cinnamaldehyde **6** in 73% yield. Bis(indolyl)methane compound **7** was obtained in 81% yield from **6** and 1-methylindole catalyzed by molecular iodine in CH<sub>3</sub>CN at room temperature. Hydrolysis of **7** with LiOH·H<sub>2</sub>O in methanol and acidification afforded the final product **8** in 91% yield (Scheme 1, HRMS *m/z* [M + H]<sup>+</sup> calcd for C<sub>26</sub>H<sub>23</sub>N<sub>2</sub>O<sub>2</sub>S 427.1480, found 427.1468) (Figure S1a). The compound was also thoroughly characterized by 1D <sup>1</sup>H (Figure S1b) and <sup>13</sup>C (Figure S1c) nuclear magnetic resonance (NMR) spectroscopy.

**Synthesis of Nano-RXR.** We introduced a strategy for synthesizing nanoscopic RXR agonists based on “rigid cored” micelles (RCMs).<sup>44–48</sup> In brief, Nano-RXR were produced by the molecular co-self-assembly of amphiphilic PS<sub>67</sub>-*b*-PAA<sub>27</sub> (polystyrene-*b*-poly(acrylic acid)) and polyoxyethylene (20) cetyl ether. (Figure 2A) In a typical procedure, polyethylene

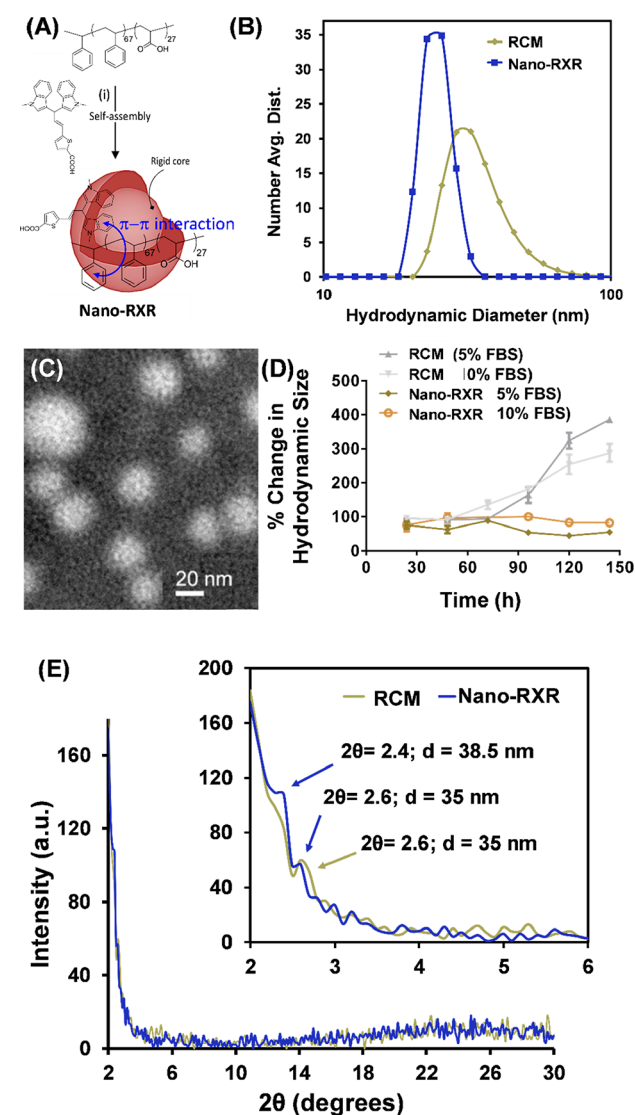


**Figure 2.** Physicochemical characterization of Nano-RXR. (A) Synthesis of rigid nanoparticles loaded with RXR-8 to prepare Nano-RXR; (B) hydrodynamic diameter of Nano-RXR compared to nanoparticles; (C) TEM image (drop deposited over carbon grid) of Nano-RXR; (D) stability of nanoparticles and Nano-RXR formulations in 5% and 10% (v/v) concentration of fetal bovine serum (FBS); (E) XRD pattern of nanoparticles and effect of RXR-8 loading in nanoassembly.

glycol cetyl ether (0.5 mg) was melted at 65 °C for 5 min, and then 1 mL of water was added dropwise while stirring the mixture. The micellar suspension was allowed to stir for 20 min at 1150 rpm. A solution of amphiphilic diblock copolymer (PS<sub>67</sub>-*b*-PAA<sub>27</sub>) and the solution of RXR-8 was prepared to achieve 2.5 mM in chloroform followed by dropwise addition to the mixture. The solution was left to stir overnight to evaporate the organic solvents; additional water was added, and the suspension was stored at 4 °C overnight for curing the core of

the particle. Arresting the core of these polymeric-based nanoassemblies reduces the flexibility of the nanoconstruct leading to a more robust arrangement for systemic administration. The characterization of Nano-RXR was performed for hydrodynamic diameter, dry state morphology, height profile, and ordered assembly.

This resulted in hydrodynamic size of Nano-RXR as 32 ± 6 nm and a bigger assembly of rigid cored micelles (RCM) at 45 ± 5 nm (Figure 2B). This sub-100 nm spheroidal anhydrous morphology of Nano-RXR was further confirmed by transmission electron microscopy and found to be ~20 ± 5 nm in the anhydrous state (Figure 2C). The stability of nanoparticles and Nano-RXR formulations in 5% and 10% (v/v) concentration of fetal bovine serum (FBS) showed greater stability of Nano-RXR compared to nanoparticles alone (Figure 2D). Retinoid X receptor (RXR) agonist ligand with a bis(indolyl)methane scaffold co-self-assembled with PS<sub>67</sub>-*b*-PAA<sub>27</sub> resulting in nanoparticles with excellent kinetic stability through π–π stacking and hydrophobic interactions. The incorporation of RXR molecules in nanoassembly was further confirmed by XRD pattern of Nano-RXR and nanoparticles (Figure 2E). It was observed that Nano-RXR showed greater order with *d*-spacing at a higher value of 38.5 nm compared to a common peak with *d* spacing of 35 nm in case of nanoparticles alone. It is likely that the incorporation of RXR agonist in the nanoassembly makes wider repeating units in Nano-RXR. This representative X-ray diffraction study revealed the incorporation of RXR agonist molecules inside intralayer arrangements of micelles. Shelf life stability (in vial) of the nanoparticles was monitored over time (0, 7, 14, and 30 days and over six months) by observing the changes in hydrodynamic diameters, zeta potential, and polydispersity, and these were found not to be changing to any considerable extent (data not shown).

**In Vitro Cell Toxicity Assay for Evaluating Efficacy of the RXR-Selective Agonist.** Cell toxicity studies were performed using MTT assay on sarcoma cells (63-3 cre and 141-10 cre) and compared with effects on their noncancerous counterparts (63-3 and 141-10) generated from Oncopig tissues (Figure 3a,b). RXR-8 and Nano-RXR were added to cultures at concentrations of RXR ranging from 3.125 to 100 μM for 48 h prior to performing the MTT assay. Empty nanoparticles were added at an equivalent amount as a negative control. Nanoparticle encapsulated RXR-8 demonstrated increased cytotoxicity over that of RXR-8 alone ( $p \leq 0.01$ ). Comparison of the effects of these agents on controls (nontransformed 63-3 and 141-10) and matched transformed cell lines (63-3 Cre and 141-10 Cre) were determined by measuring half-maximal inhibitory concentrations (IC<sub>50</sub>). The observed maximum effects of Nano-RXR treatment in 63-3 Cre with minimum IC<sub>50</sub> value was 44 ± 2.2 compared to 38 ± 2.5 μM in the case of 141-10 Cre. To evaluate the selectivity of Nano-RXR toward sarcoma cells, MTT assays were also performed in noncancerous cells of same origin, 63-3 and 141-10. It was found that IC<sub>50</sub> for Nano-RXR in 63-3 was significantly higher ( $p = 0.001$ ) at 70 ± 3.5 compared to 44 ± 2.2 in 63-3 Cre (Figure 3a) and 100 ± 5 μM for 141-10 compared to 38 ± 2.5 μM in 141-10 Cre ( $p = 0.0001$ ) (Figure 3b). These evaluations reveal not only a greater toxicity response for Nano-RXR compared to free RXR in sarcoma cells but elevated selectivity against noncancerous cells of same origin.

**Oncopig Cancer Model of Soft Tissue Sarcoma.** The Oncopig cancer model (OCM) was developed as a model of human disease because pigs are similar in size, anatomy,

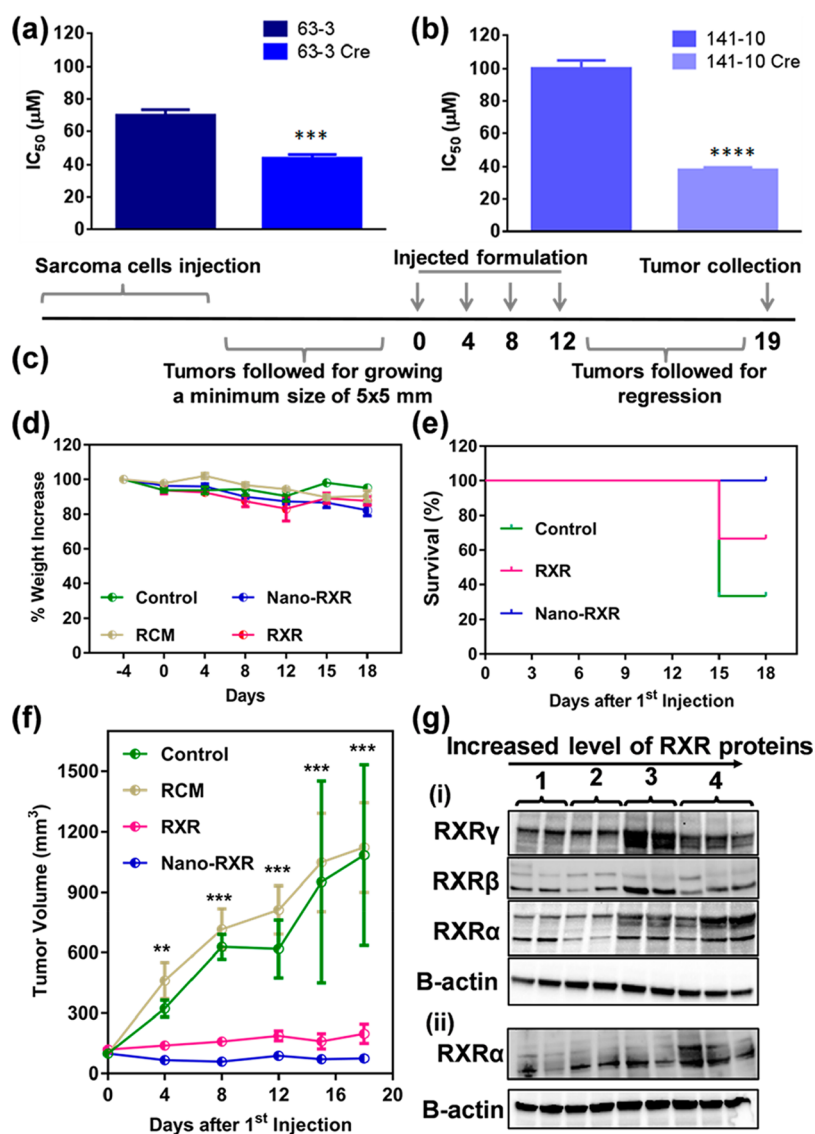


**Figure 3.** Cytotoxic effect of Nano-RXR and RXR on porcine sarcoma cell lines. RXR and Nano-RXR were used at various concentrations of RXR ranging from 3.125 to 100  $\mu\text{M}$  for 48 h before performing the MTT assay. Nanoparticles alone at equivalent amount were used as negative control to evaluate the safety pattern of nanoparticles in the same conditions. Biostatistical analysis showed nanoparticle-based improvement enhanced cell growth inhibition with  $p$  value of 0.01 as \*\*. As an indication of cytotoxic selectivity with lowering in  $IC_{50}$  values, Nano-RXR showed statistically lower  $IC_{50}$  in (a) 63-3 Cre and (b) 141-10 Cre cells compared to that in noncancerous cells of the same origin, 63-3 and 141-10, respectively.  $p$  Values of 0.001 and 0.0001 are shown as \*\*\* and \*\*\*\*, respectively, as obtained after unpaired  $t$  test. In vivo tumor regression studies in mouse and subsequent effects on protein expression. (c) Timeline of the in vivo experiment in rodent xenograft model; (d) weight percentages of group of animals used for tumor regression studies; (e) survival (%) of group of animals treated with RXR or Nano-RXR compared to controls on 18th day of experiment; (f) tumor volume regression after treatment with RXR and Nano-RXR; nanoparticles alone (RCM) or untreated animals were used as controls; (g) protein expression in tissues collected from treated and untreated groups of animals: (1) buffer; (2) RCM; (3) RXR; (4) Nano-RXR as obtained from (i) tumor tissue and (ii) tissue collected from liver.

metabolism, and genetics compared to humans. This line of pigs carries an inducible KRASG12D and TP53R167H transgene, allowing for soft tissue sarcoma modeling in a spatial and temporal manner.<sup>50,43</sup> This study utilized both Oncopig soft tissue sarcoma cell lines (fibroblast origin) and in vivo tumors (leiomyosarcoma). Both of these have been shown to have similar transcriptional alterations as do human STS including altered TP53 signaling, Wnt signaling activation, and some master regulators such as FOSL1 which have been identified as potential therapeutic targets.<sup>50</sup>

#### In Vivo Tumor Regression in Rodent Using Nano-RXR.

An in vivo study to evaluate the effects of RXR-8 and Nano-RXR on tumor growth was completed utilizing a porcine tumor cell

xenograft into SCID mice. The tumorigenic sarcoma line 63-1 (sarcoma cells) was injected subcutaneously into two sites per mouse. When tumors reached approximately  $5 \times 5$  mm, each tumor was injected with buffer, RCM, RXR-8, or Nano-RXR (total four injections, on day 0, 4, 8, and 12 with 40  $\mu\text{L}$  containing RXR-8 concentration of 62.5  $\mu\text{g}/\text{mL}$ ), and tumor volume was monitored by caliper measurements through day 35 before euthanization of the animals (Figure 3c). Body weight measurement of mice revealed no significant loss in any group (Figure 3d). Treatment with either RXR-8 or Nano-RXR increased survival time of the mice and retarded the tumor volume when compared to untreated animals or those receiving nanoparticles alone (RCM). Treatment with Nano-RXR was

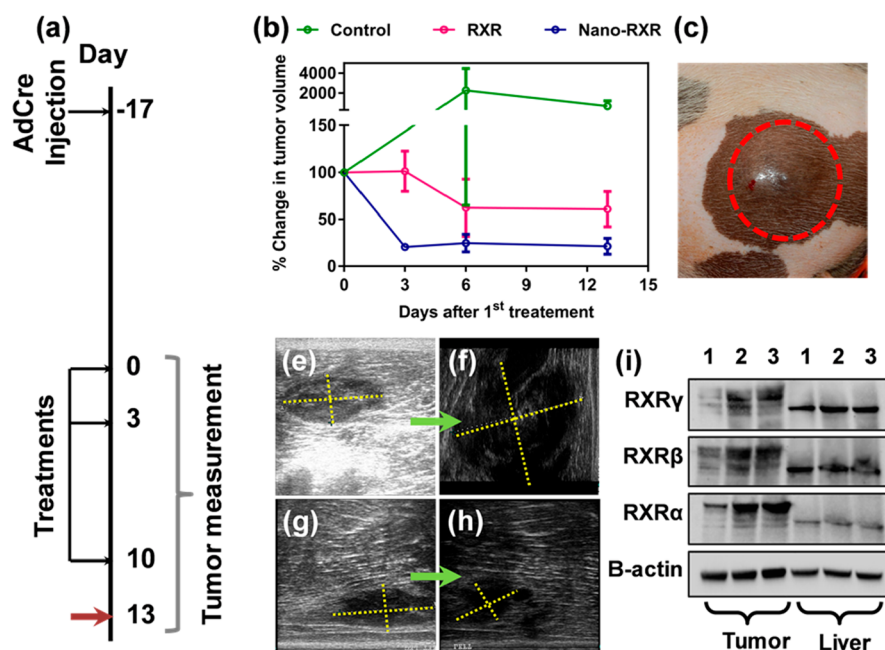


**Figure 4.** In vivo tumor regression studies in pig and post-treatment effects on protein expression. (a) Timeline of in vivo experiment in onco-pig model. (b) Tumor appearance on day 1 of buffer injection. (c) Tumor volume regression after treatment with RXR and Nano-RXR; animals treated with buffer were used as controls. Ultrasound imaging to follow the tumor growth after treatment with buffer on (d) day 1 and (e) day 13 and animals treated with Nano-RXR on (f) day 1 and (g) day 13. (h) Protein expression in tissues collected from treated and untreated group of animals: (1) Buffer; (2) RXR; (3) Nano-RXR as obtained from tumor tissue and tissue collected from liver.

more effective in reducing tumor volume compared to RXR-8 alone (Figure 3f). Protein expression analysis clearly showed the upregulation of RXRs with maximum effect in level of RXR $\alpha$  and RXR $\beta$  for collected tumors at the end of the tumor regression experiment, while effects were minimal in liver tissue collected from the same animals (Figure 3g).

**Safety Profile and Tumor Regression Efficiency in Pig Model.** It was observed that none of the formulations at these doses (4 mL; 0.5 mg of RXR/kg) produced any significant toxic changes in any of the clinical chemistries of the Oncopigs treated (Table S1). A transient increase in CPK, total bilirubin, and glucose were seen following the treatments, which returned to normal with longer time interval (24 h). Histopathological evaluations performed on various organ tissues collected from these animals were found to be within normal animal variations (See details in Supporting Information). To study the tumor regression efficiency, the volume of the tumors was determined from ultrasound images after different treatments. On day 0 (17 days after AdCre injection), a single tumor on each animal was injected with either buffer, RXR-8, or Nano-RXR, which was followed by 2 additional injections on days 3 and 10 (1 mL volume of 62.5  $\mu$ g/mL). The tumor size was evaluated for 13 days after the first injection (Figure 4a). Tumors were first identified based on palpation and visual inspection (Figure 4b) and then by ultrasound (US) imaging. Tumor sizes were visualized by US imaging; tumor (Figure 4d) treated with buffer alone continued to grow until the end of the study (Figure 4e), whereas tumor (Figure 4f) treated with Nano-RXR had significantly retarded growth (Figure 4g).

Further US imaging was done to accurately identify the treatment region so that tissue was dissected appropriately for gross pathology and histology analysis. The tumor volume was found to be significantly ( $p < 0.001$ ) lower following RXR-8 or Nano-RXR treatment when compared to buffer (Figure 4c). Nano-RXR was more effective compared to RXR-8 alone.

Animals were inspected daily for body weight and behavioral changes and showed no change. At day 13, immediately after imaging, animals were euthanized; tumors were resected and weighed, and half of the tissue was snap frozen in liquid N<sub>2</sub> prior to storage at  $-80^{\circ}\text{C}$ , while other half was put in formalin (10%). Formalin samples were harvested for histopathological analysis. The treatment region plus boundary (1–2 cm) was dissected and used for the pathological analysis. Frozen samples were used for extracting RNA and protein for expression studies. Protein expression analysis clearly showed the upregulation of RXRs with maximum effect on levels of RXR $\alpha$  and RXR $\gamma$  for collected tumors at the end of the tumor regression experiment, while effects were minimal in liver tissues collected from the same animals (Figure 4h).

Expression of protein from tumor post-treatment in animal models gives additional proof for the activity of small molecule and nanotherapeutics through certain cellular cascades. An extensive protein expression analysis was performed on tumors collected from the mouse model post-treatment and sacrifice. RXR protein level was found to increase significantly ( $p < 0.05$ ) post-Nano-RXR treatment compared to RXR-8 or nanoparticles. Protein level changes were noted to be maximal for RXR $\alpha$ , while RXR $\beta$  and RXR $\gamma$  showed little or no effect. Protein expression was also measured in liver tissue of the treated animals, and it was found that the expression levels were not significantly different across different treatment groups. This signifies that the RXR agonist mediated upregulation of RXR $\alpha$  in the animal model for tumor tissues causing tumor regression as an after effect. Effect and side effects<sup>49</sup> of Nano-RXR treatment in Oncopigs were evaluated by post-treatment necropsies and histopathology (see details in Supporting Information).

**Differential Expression of Drug Metabolism, Regulation, and Transport Genes.** Differential gene expression was studied for genes involved in drug metabolism, regulation, and transport. Drug clearance and pharmacokinetics are highly

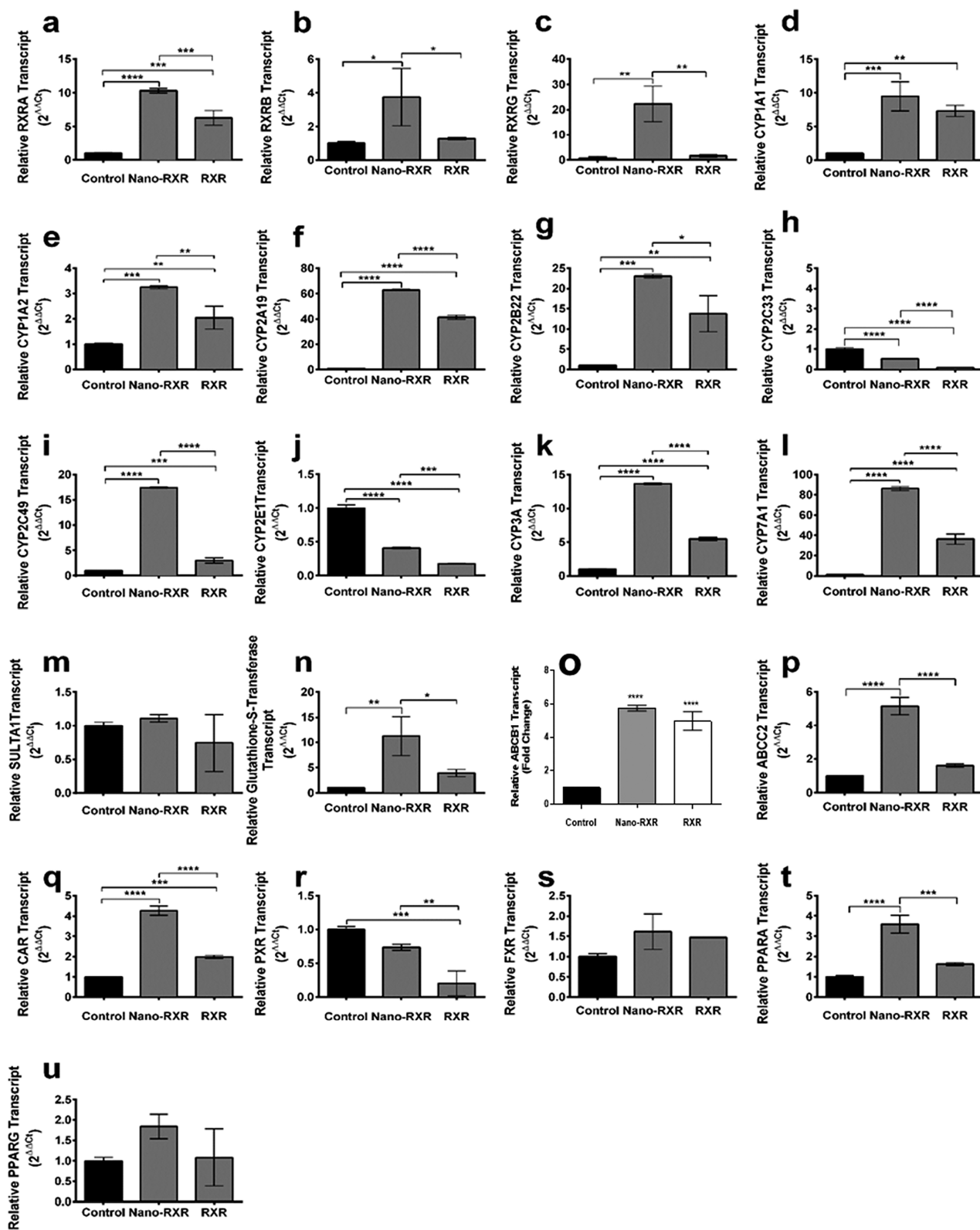


**Figure 5.** RXR and Nano-RXR induced transcriptional alteration of genes involved in phase-I and phase-II drug metabolism, phase-III transport, and nuclear receptors in liver measured by qPCR. Real time (RT)-PCR was performed to analyze the expression of the 21 genes. Fold change in transcript upon RXR or Nano-RXR treatment is presented with respect to control. CYP2C33, CYP2E1, and PXR were downregulated, SULTA1, FXR, and PPAR $\gamma$  were unchanged, and the rest of the genes were upregulated. The values and error bars represent average and standard deviations of three independent sets of experiments. One-way analysis of variance (ANOVA) followed by Bonferroni post-test was performed to determine significant differences among control and treatments. *p* Values of 0.05, 0.01, 0.001 and 0.0001 are shown as \*, \*\*, \*\*\*, and \*\*\*\*, respectively.

regulated by the drug metabolism route, which in turn can affect the clinical efficiency and drug toxicity.<sup>50,51</sup> During metabolism

of drug, it undergoes two phases: Initially, in phase I, the drug experiences oxidation due to the oxidative pathways and

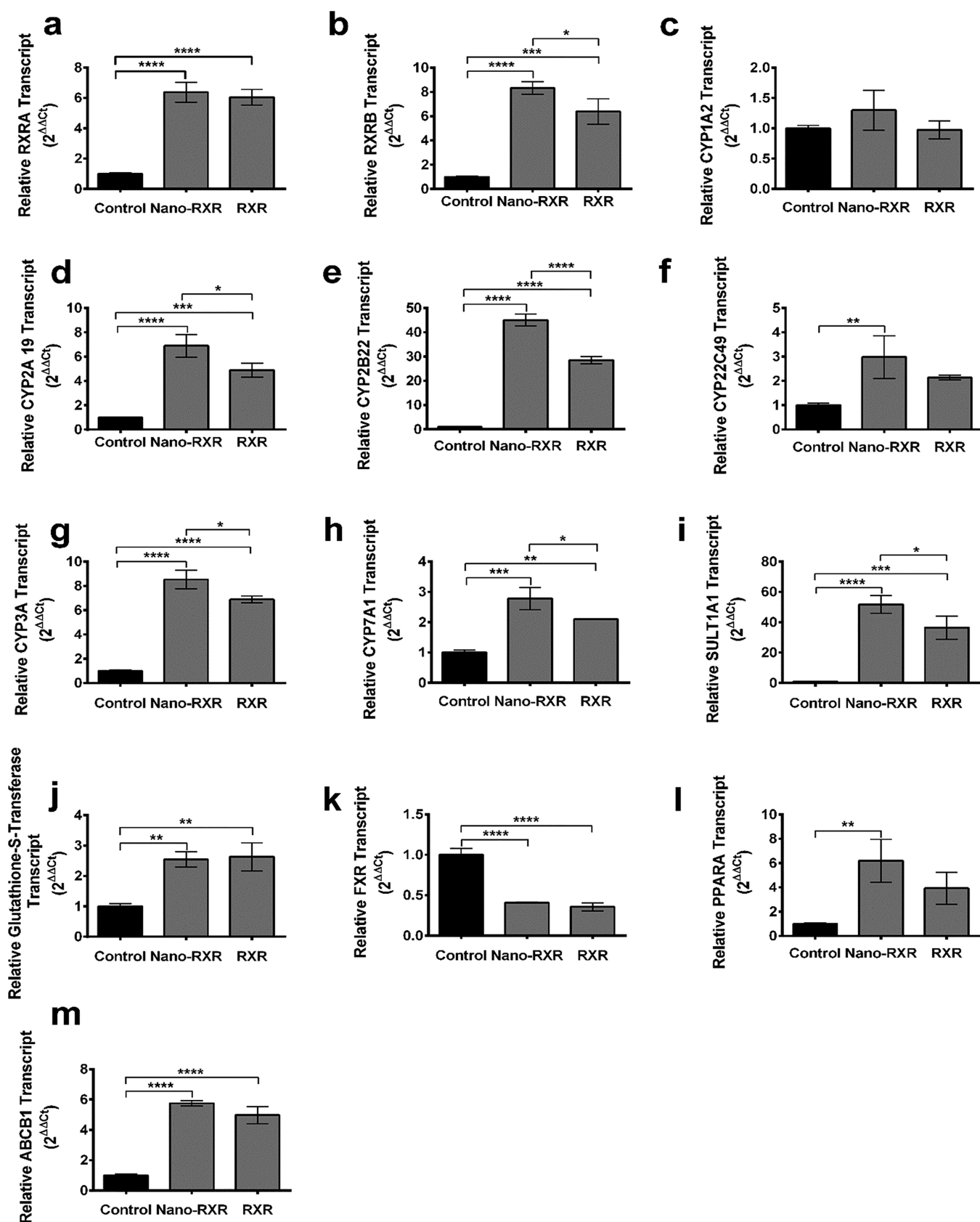


**Figure 6.** RXR and Nano-RXR induced transcriptional alteration of genes involved in phase-I and phase-II drug metabolism, phase-III transport, and nuclear receptors in tumor measured by qPCR. Real time RT-PCR was performed to analyze the expression of the 21 genes. Fold change in transcript upon RXR or Nano-RXR treatment is presented with respect to control. FXR was downregulated, CYP1A2 was unchanged, and all the other genes were upregulated by treatment. The values and error bars represent average and standard deviations of three independent sets of experiments. One-way analysis of variance (ANOVA) followed by Bonferroni post-test was performed to determine significant differences among control and treatments. *p* Values of 0.05, 0.01, 0.001 and 0.0001 are shown as \*, \*\*, \*\*\*, and \*\*\*\*, respectively.

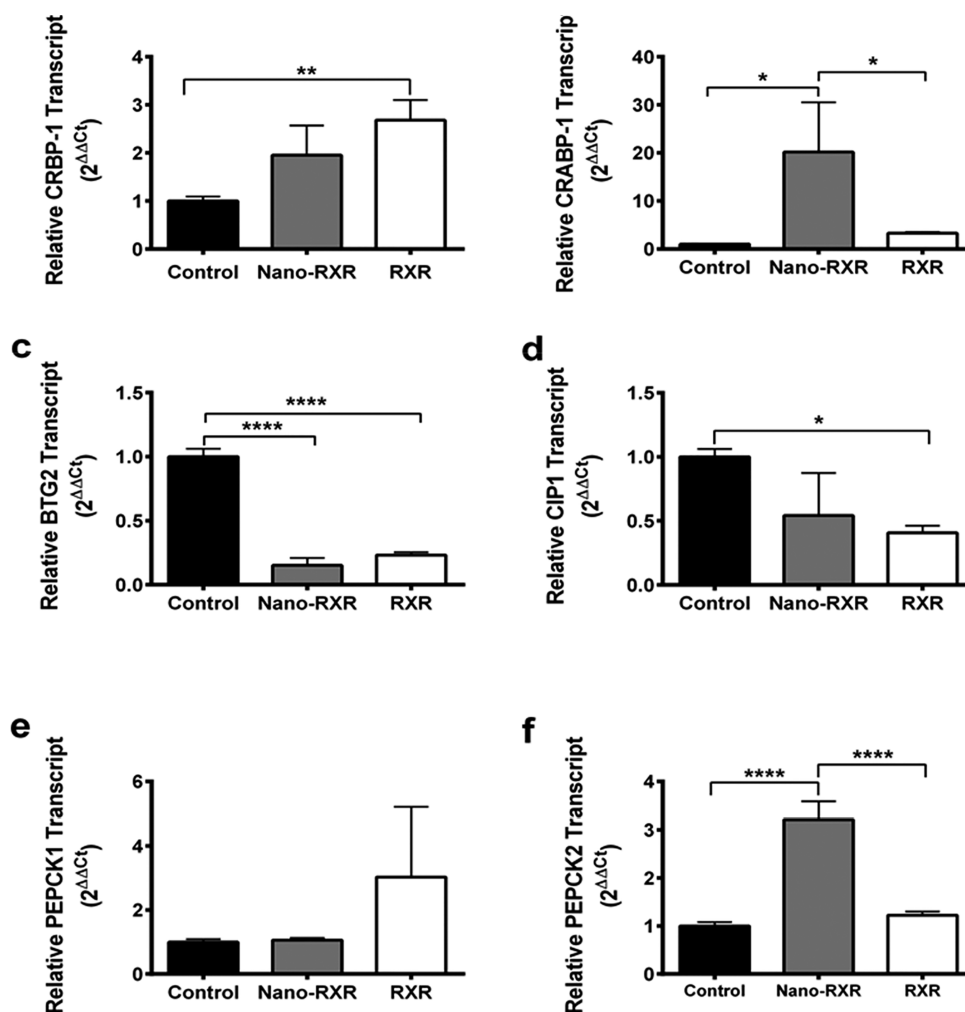


**Figure 7.** (a–e) RXR and Nano-RXR induced transcriptional alteration of downstream target genes measured by qPCR. Real time RT-PCR was performed to analyze the expression of the six genes. Fold change in transcript upon RXR or Nano-RXR treatment is presented with respect to control. CRBP-1, CRABP-1, PEPCK1, and PEPCK2 were upregulated, and BTG2 and CIP1 were downregulated by treatment ( $n = 3$ ). One-way analysis of variance (ANOVA) followed by Bonferroni post-test was done to determine significant differences among control and treatments where  $n = 3$ .  $p$  Values of 0.05, 0.01, 0.001 and 0.0001 are shown as \*, \*\*, \*\*\* and \*\*\*\*, respectively.

therefore becomes more a polar substance. Specifically, cytochrome P450 (CYP) monooxygenases, a major class of membrane-associated heme proteins, have an essential role in exerting oxidative metabolism in a wide gamut of xenobiotics and endogenous compounds.<sup>52</sup> P450 enzymes responsible for drug metabolism have been extensively studied in pig liver, and it was determined that the main subcategories are 1A1, 1A2, 2A19, 2C33, 2C49, 2E1, 3A, and 7A1.<sup>53–55</sup> On the other hand, in phase II metabolism, conjugation with hydrophilic compounds occurs, which leads to improved polarity and water solubility. This would ultimately increase the chances of excretion in bile and urine for detoxification.<sup>56,57</sup> Toward this, we identified genes responsive to the treatment of ligand Nano-RXR and RXR-8, including orphan nuclear receptors (regulators), RXR $\alpha$ , RXR $\beta$ , RXR $\gamma$ , CAR, PPAR $\alpha$ , PPAR $\gamma$ , FXR, pregnane X receptor (PXR), genes involved in phase I drug metabolism (oxidation reactions), for example, CYP1A1, CYP1A2, CYP2A19, CYP2B22, CYP2C33, CYP2C49, CYP2E1, CYP3A, and CYP7A1, and genes involved in phase II drug metabolism (conjugation reactions), for example, glutathione-S-transferase, SULTA1, and transporters such as ABCB1 and ABCC2. Significant upregulation (3–20-fold) of all the three isoforms

of RXR was observed in treated porcine livers over that of control liver (Figures 5–7). Nuclear hormone receptors, namely, the farnesoid X receptor (FXR), the liver X receptors (LXRs), and the peroxisome proliferator-activated receptors (PPARs) are a class of ligand-activated transcription factors involved in regulation of hepatic lipid metabolism.<sup>58</sup> There are several biological processes that are regulated in liver, such as bile acid synthesis and metabolism, lipoprotein metabolism, lipogenesis, and fatty acid degradation, controlled by these hormones. Moreover, they turn on the gene transcription when complexed with the retinoid X receptor, RXR, and next by activation of the heterodimeric complex to initiate the response elements in the DNA.<sup>59</sup> It was found that ligand Nano-RXR and RXR-8 both could induce overexpression of PPAR $\alpha$  (Figure 5t), and PPAR $\gamma$  (Figure 5u) and FXR (Figure 5s) showed no significant change, whereas LXR (Figure 5r) showed significant decrease in gene expression.

Transcript levels of all the three RXR isoforms were higher in Nano-RXR treated liver than RXR-8 treated liver. All the studied genes except CYP2C33 and CYP2E1, which were involved in phase I drug metabolism, were upregulated in ligand treated livers when compared to that of control liver. Significant

difference between Nano-RXR and RXR-8 was observed for most of the genes involved in phase I drug metabolism. Whereas glutathione-S-transferase was significantly upregulated in ligand treated groups compared to the control group, no difference in transcript level of SULTA1 was observed among the groups. The mRNA levels of two transporters (ABCB1, ABCC2) were increased in treated liver over that of control liver for both treatment with RXR-8 and Nano-RXR with higher effect in the case of Nano-RXR (Figure 5o). CAR and PPAR $\alpha$  were upregulated in ligand treated groups compared with control; no differences in FXR and PPAR $\gamma$  were observed, and PXR was downregulated in treated groups. This clearly confirms the involvement of ligand Nano-RXR and RXR-8 through RXR and other gene cascade pathways of the porcine liver.

**Differential Expression of Drug Metabolism, Regulation, and Transport Genes from Control and Treated Tumor Tissues.** We also studied the differential gene expression of genes that are involved in drug metabolism, regulation, and transport in treated and control tumor tissues. The expression of RXR $\gamma$ , CYP1A1, CYP2C33, CYP2E1, CAR, PXR, PPARG, and ABCC2 was not detected in control tumor. The differential expression patterns of the other genes were similar to that of liver mentioned above. Significant upregulation in RXR $\alpha$  and  $\beta$  was observed in ligand treated tumors in comparison to control tumor. In case of genes involved in phase I drug metabolism, all the studied genes except CYP1A2 were upregulated in treated groups compared to control group. The two genes involved in phase II drug metabolism (SULTA1 and glutathione-S-transferase) and transporter ABCB1 were upregulated in treated groups. PPAR $\alpha$  was upregulated but FXR was downregulated in treated groups compared with control group.

**Effect of Nano-RXR and RXR-8 on Downstream Target Genes in Liver.** In the present study, we have analyzed the differential expression of six downstream target genes of RXR, CRBP-1, CRABP-1, BTG2, CIP1, PEPCK1, and PEPCK2, in liver samples from control pigs and Nano-RXR and RXR-8 treated Oncopigs. Upregulation of CRBP-1, CRABP-1, PEPCK1, and PEPCK2 were observed in treated liver whereas BTG2 and CIP1 were downregulated (Figure 5). Significant difference between Nano-RXR and RXR-8 was found in CRABP-1 and PEPCK2.

The heterodimer of RARs with RXRs works as a transcription factor to regulate the target genes of RA. They tend to bind to DNA sequences called RA-response elements localized with the promoter of target genes.<sup>60</sup> Cellular retinol binding protein 2 and fatty acid binding protein 5 are responsible for the partitioning of RAs between the two receptors. These proteins specially deliver RAs from the cytosol to nuclear RAR and RXR, followed by the activation of a variety of downstream target genes like upregulation of CRBP-1, PEPCK, and CRABP-1 after RXR treatment.

It has recently been demonstrated that retinoids regulate the gene for the gluconeogenic enzyme, cytosolic phosphoenolpyruvate carboxykinase (PEPCK, EC 4.1.1.32), in liver.<sup>61–64</sup> One of the target genes that RAR and RXR family would bind to are the ones encoding cytosolic PEPCK. It contains specific retinoic acid response elements (RAREs) in the 5'-flanking sequence.

CIP1 encodes a potent cyclin-dependent kinase inhibitor and inhibits the activity of cyclin-cyclin-dependent kinase 2 or -cyclin-dependent kinase 4 complexes. As a result of this activity, CIP1 functions as a regulator of cell cycle progression at G1. The tumor suppressor protein p53 tightly controls the

expression of this gene and helps to mediate the p53-dependent cell cycle G1 phase arrest under various stress stimuli.

## CONCLUSION

We present an “in silico to in vivo” approach to discover, synthesize, and deliver highly potent payloads of retinoid-selective receptor (RXR) agonists specifically to sarcoma cells while minimizing off-target effects and toxicity by nanoparticle-enabled delivery. RXR-selective agonists were identified through structure-based drug discovery involving computational modeling studies for transcriptional activation of orphan nuclear receptor. The chemical synthesis of the agent was accomplished followed by inclusion of these molecules into stable micellar particles for nanoenabled delivery. Once the in vitro efficacy was established, a holistic approach was adopted to establish their potency first in a mouse model and then in a translational transgenic Oncopig cancer model of sarcoma.<sup>65</sup> Oncopig represents a genetically malleable large animal model with high similarity of anatomy, physiology, metabolism, and genetics to human. To our knowledge, a study to evaluate actual tumor treatment response to RXR therapy in a large animal has never been done due to the lack of an appropriate tumor model. Our results suggest that this agent induced modulations of expression of RXR related genes in tumor as well as in liver of treated animals including rodents and Oncopigs. As RXR forms a heterodimer with other orphan nuclear receptors to induce expression of drug metabolism genes, the expression of several other nuclear receptors also increased. A significant upregulation of phase I drug metabolism genes (CYP isoforms) also was reported with a few exceptions supporting the no-retention possibility of newly synthesized drug molecule RXR-8 and negating the possibility of retention related toxicities in subjects. In general, the Nano-RXR was more effective than the RXR-8 drug alone in tumor regression, gene expression, and protein modulation. We anticipate that outcome of this work would have a necessary advancement of significant translational impact to achieve the survival of patients with soft tissue sarcoma.

## EXPERIMENTAL SECTION

**Materials.** Unless otherwise mentioned, all chemicals and reagents were obtained from Sigma-Aldrich, Inc. (St. Louis, MO), and used with no more purification. The hydrodynamic diameter was measured on a Malvern Zetasizer instrument operating with a 633 nm laser. Zeta potential measurement was done on a Malvern Zetasizer instrument (Nanoseries, Malvern Instruments Ltd., United Kingdom). The TEM images were acquired on a JEOL 2100 Cryo TEM using Gatan UltraScan 2k  $\times$  2k CCD. The XRD data was collected on instrument Siemens-Bruker D5000 diffractometer and analyzed using software Jade X-ray analysis. The absorbance reading of MTT cell viability assay was done on a plate reader (Synergy HT, Bio-Tek). Bright field imaging was done using microscope DMI3000 B, Leica Microsystems, Buffalo Grove, IL.

**Structure-Based Design, Lead Optimization, and Synthesis of RXR Agonists.** In order to identify the better RXR agonist with high binding affinity and selectivity, hydrogen bond, ion-salt, and hydrophobic interactions of the bis(indolyl)methane framework and globular shape of RXR were fine-tuned as depicted in Figure 1c–f. Changes in structural units were made at the bridge region, hydrophobic end, and carboxylic acid end: (1) phenyl instead of thiophene; (2) hydrogen and isopropyl instead of methyl; (3) 2,4-thiazolidinedione instead of carboxylic group. Three-dimensional structures of prospective DIM-arenes were constructed using the SKETCH module in Sybyl 7.1 (Tripos, St. Louis, MO, USA). Energy was minimized with the Tripos force-field using the conjugated gradient method until a convergence value of 0.005 kcal/mol was achieved. Subsequently, docking was

performed on docking program AutoDock 4.0. A 50 point grid map in the  $x$ ,  $y$ , and  $z$  directions was created using the Arg316 residue of the RXRa LBD (PDB code 1MVC) as the central residue and 0.375 as the grid spacing. A distance-dependent function of the dielectric constant was used for the energetic map calculations. In order to identify the ligand's torsion angle, the AutoDockTools suite was utilized, and Gasteiger and Kollman partial atomic charges to DIM-arenes and the RXRa LBD were assigned, respectively. One hundred independent docking runs were performed for each DIM-arene using the Lamarckian genetic algorithm and a maximum number of 2 500 000 energy evaluations. Other parameters were assigned default values, implemented by the program. Cluster analysis performed on the results from 100 runs gave a root-mean-square tolerance of 2, validating the significance of the program.

**Synthesis of Bis(indolyl)methane-based RXR Agonist. Synthesis and Characterization of 6 (Precursor).** To a stirred solution of **5**, ethyl 5-bromothiophene-2-carboxylate (352.7 mg, 1.5 mmol), in 10 mL of DMF were added acrolein diethyl acetal (585 mg, 4.5 mmol),  $n\text{Bu}_4\text{NOAc}$  (862 mg, 3 mmol),  $\text{K}_2\text{CO}_3$  (310.5 mg, 2.25 mmol), KCl (111.8 mg, 1.5 mmol), and  $\text{Pd}(\text{OAc})_2$  (10.1 mg, 0.045 mmol). The mixture was stirred for 1.5 h at 90 °C. After cooling, 2 N HCl was slowly added, and the reaction mixture was stirred at room temperature for 10 min. Then, it was diluted with EtOAc and washed with water. The organic layer was dried over  $\text{Na}_2\text{SO}_4$  and concentrated under reduced pressure. The residue was purified by chromatography (hexane/EtOAc 8:1) to give the product as a white solid (255 mg, 81% yield). HRMS:  $m/z$   $[\text{M} + \text{H}]^+$  calcd for  $\text{C}_{10}\text{H}_{11}\text{O}_3\text{S}$  211.0429, found 211.0429.

**Synthesis and Characterization of RXR-8.** Aldehyde (210 mg, 1.00 mmol), 1-methylindole (262 mg, 2.00 mmol), and  $\text{I}_2$  (25.38 mg, 0.1 mmol) in MeCN (3 mL) was stirred for 2 h, at which time TLC indicated complete reaction. The mixture was treated with 5%  $\text{Na}_2\text{S}_2\text{O}_3(\text{aq})$  (5 mL) and extracted with EtOAc (3  $\times$  5 mL). The extract was washed ( $\text{H}_2\text{O}$  and brine) and dried. Concentration and chromatography (33% EtOAc/hexane) afforded **7** as a tan solid (36.83 mg, yield: 81%) HRMS:  $m/z$   $[\text{M} + \text{H}]^+$  calcd for  $\text{C}_{28}\text{H}_{27}\text{N}_2\text{O}_2\text{S}$  455.1793, found 455.1784. Lithium hydroxide monohydrate (21 mg, 0.5 mmol) was added to a solution of **7** (45.46 mg, 0.1 mmol) in MeOH. This mixture was heated at reflux under nitrogen for 3 h, cooled to room temperature, acidified with 1 N HCl, and extracted with EtOAc. The extract was washed ( $\text{H}_2\text{O}$  and brine). Concentration and drying gave the pure carboxylic acid (RXR-8) as tan solid (38.8 mg, yield 91%). HRMS:  $m/z$   $[\text{M} + \text{H}]^+$  calcd for  $\text{C}_{26}\text{H}_{23}\text{N}_2\text{O}_2\text{S}$  427.1480, found 427.1468. Elemental analysis: calcd for  $\text{C}_{26}\text{H}_{23}\text{N}_2\text{O}_2\text{S}$  C 73.21%, H 5.2%, and N 6.57%; found C 73.42%, H 5.52%, and N 7.06%. From the elemental analysis results, purity of the compound RXR-8 was found to be  $\geq 95\%$ .

**Dynamic Light Scattering.** Average hydrodynamic diameter distributions for Nano-RXR were determined using a Malvern Zetasizer nanoseries, Nano ZS90, with fixed angle of 90°. The stability of the nanoparticles was assessed by measuring the hydrodynamic diameter at 0, 24, 48, 72, 96, and 120 h postsynthesis ( $n = 5$ ).

**Zeta Potential Determination.** Zeta potential ( $\zeta$ ) values for the Nano-RXR formulations were determined with a nanoseries Malvern Zetasizer zeta potential analyzer. The data for the dialyzed nanoparticles (MWCO 20 kDa dialysis tubing, Spectrum Laboratories, Rancho Dominguez, CA) was collected in the phase analysis light scattering (PALS) mode using the Smoluchowski equation for  $\zeta$  potential determination. The mean and SD value of 10 data accumulations were reported.

**Transmission Electron Microscopy.** To observe the morphology of Nano-RXR, transmission electron microscopy (TEM) was performed. The sample was deposited on a carbon coated Cu grid and negatively stained with uranyl acetate.

**X-ray Diffraction Studies.** The ordered behavior of Nano-RXR was determined by X-ray diffraction measurement. The aqueous suspension of each formulation was drop cast on a microscopic glass slide and fully dried. X-ray diffraction (XRD) of was performed using the  $\theta$ - $2\theta$  configuration on a Siemens-Bruker D5000 diffractometer. The X-ray beam was generated with a Cu anode, and the Cu  $K\alpha$  beam of

wavelength 1.5418 Å was used for the experiments. Scans were performed for  $2\theta$  range of 2 to 50.

**MTT Assay.** The cytotoxic effects of RXR and Nano-RXR were evaluated on control porcine fibroblast lines (63-3, 141-10) and compared with matched transformed (AdCre treated 63-3 Cre, 141-10 Cre) sarcoma cell lines. The in vitro cytotoxicity was determined by the MTT assay.<sup>66</sup> Tetrazolium MTT (3-(4, 5-dimethylthiazolyl-2)-2,5-diphenyl-tetrazolium bromide) is converted to purple formazan crystals as a result of dehydrogenase enzymes in the metabolically active cells.<sup>67</sup> The salt was solubilized in DMSO, and the absorbance at 570 nm was recorded. For the MTT assay, cell lines were seeded in a 96 well plate ( $1 \times 10^4$  cell/well) in basal medium, and after 24 h of adherence, the cells were treated with various concentrations (0 to 100  $\mu\text{M}$ ) of RXR and Nano-RXR and incubated for another 48 or 72 h at 37 °C in an atmosphere of 5%  $\text{CO}_2$  in air. At the appropriate time, the medium was removed, 200  $\mu\text{L}$  of PBS was used to wash the cells, and 100  $\mu\text{L}$  MTT solution (1 mg/mL) was added to each well followed by incubation for 4 h under condition mentioned above. Then the MTT containing media was removed, and the formazan crystals were dissolved with 200  $\mu\text{L}$  of DMSO. Absorbance was measured at 570 nm using microplate reader.

**AdCre Induction of Tumors in Pigs.** All animal studies and procedures were approved by the University of Illinois IACUC. Under sedation, Oncopigs were injected intramuscularly (IM) in the upper part of left and right legs. Ad5CMVCre-eGFP (AdCre) (Gene Transfer Vector Core, University of Iowa) was diluted with minimal essential medium (MEM, GIBCO) to a final concentration of  $2 \times 10^9$  PFU/mL, and 2 mM calcium chloride (to a final concentration of 0.01 M) was added, mixed, and allowed to incubate at room temperature for 15 min prior to injection. All injections were completed before 45 min of incubation, injection sites were monitored daily, and ultrasound measurements were made on day 10 postinjection. Ultrasound imaging and palpation were used to monitor the growth of the tumor following injection.

**RXR and Nano-RXR Treatments in Oncopigs.** Beginning on day 0 (17 days post-AdCre-injection), the animals were sedated, and tumors were imaged by ultrasound to accurately measure and to guide needle placement to ensure that the therapy was administered directly into the tumor. Each animal was treated with a 1 mL volume of 62.5  $\mu\text{g}/\text{mL}$  of RXR or RXR in the form of Nano-RXR or 1 mL of saline directly into tumors. These measurements and treatments were repeated on days 3 and 10. On day 13, the animals were euthanized, and full gross necropsies were performed. Tissues were collected in 10% neutral buffer formalin for histopathology.

**Safety of RXR, Nano-RXR, and Nanoparticles in Pigs.** Side effects generated by various nanoparticle mediated drug delivery treatments are always one of the major concerns in moving forward with a therapy and are best investigated in large animal models prior to clinical trials. We performed an initial safety profile study using primary histopathology to assess toxic changes using primary histopathology from the drug (RXR-8) or nanoparticle loaded drug treatments. The initial safety profile study was conducted to assess toxic side effects in various organs using histopathology and serum chemistry. Four 4 month old male pigs weighing approximately 68 kg/each were treated with saline, nanoparticles, RXR and Nano-RXR (4 mL; 0.5 mg of RXR/kg). Serum samples were collected at 1 h and 24 h postinjection. Animals were euthanized 30 days postinjection. Pentobarbital was administered at a dose of 100 mg/kg IV into the jugular vein of pig to sacrifice the animals. For each animal, a full range of organ samples was collected and fixed in neutral buffered 10% formalin for examination by light microscopy.

**Quantitative Real-Time PCR.** Total RNA was isolated from porcine liver tissue and tumor using RNeasy Mini Kit (Qiagen) according to manufacturer's protocol. RNA pellets were dissolved in nuclease-free water and stored at  $-80$  °C until analysis. Quality of the RNA was determined by using a Nano Drop spectrophotometer and analyzed by an Agilent 2100 Bioanalyzer using an RNA Nano bioanalyzer chip to determine RNA integrity as well as the presence of absence of gDNA by the Carver High-Throughput DNA Sequencing and Genotyping Unit (HTS lab, University of Illinois, Urbana, IL,

USA). Only RNA samples with an RNA integrity number (RIN) greater than 7 were used for the study. The concentration of the RNA was determined by Qubit RNA HS Assay Kit (Thermo Fisher Scientific, Life Technologies) as per manufacturer's protocol.

Reverse transcription of RNA was performed from 1  $\mu$ g of total RNA in the presence of RNase inhibitor, random hexamer primers (50 ng/ $\mu$ L), deoxynucleotides (dNTPs, 10 mM), SuperScript III reverse transcriptase (200 U/ $\mu$ L), and reverse transcriptase buffer in a 20  $\mu$ L final reaction volume using SuperScript III First-Strand Synthesis System for RT-PCR kit (Invitrogen, Life Technologies, IN, USA).

Relative quantification of the genes was performed using Power SYBR green PCR Master Mix (2 $\times$ ) (Applied Biosystems) in Taqman ABI 7900 Real-Time PCR system (Applied Biosystems). The housekeeping genes GAPDH and  $\beta$ -actin were used as endogenous controls to normalize for RNA loading or differences in reverse transcription efficiency. The specificity of all primer pairs was checked by melting curves of the amplified products. In order to calculate the primer efficiency, each gene was first amplified in five scalar dilutions (1:10 v/v) of a control cDNA.  $C_t$  values of each dilution were plotted against the arbitrary number of copies, and the slope of the resulting linear graph was utilized to calculate the efficiency. Amplification reaction efficiency of each sample was checked to be similar to or higher than 1.6. The relative expression levels were calculated with respect to the normalized expression of the controls by delta delta  $C_t$  ( $\Delta\Delta C_t$ ) method.

**Statistical Analysis.** Statistical significance of differences between control and test samples was evaluated using one-way or two-way ANOVA using GraphPad Prism 5.0 with Bonferroni post-test analysis as applicable. Results were considered statistically significant when the  $p$  value was less than 0.05 and represented as \*, \*\*, and \*\*\*\* for  $p$  values of <0.05, 0.01, and 0.001, respectively.

**Histopathological Analyses on Oncopig Tissues after Nano-RXR Treatments.** Microscopic diagnoses revealed that most lesions within these piglets are background lesions. Mild chronic interstitial nephritis was only present in pigs that received RXR agonist and Nano-RXR. Ovarian zona granulosa apoptosis in RXR and Nano-RXR treated pigs is likely an incidental background lesion. A free RXR drug treated animal had a focal myocardial degeneration, which could be secondary to intracardiac euthanasia. Cardiotoxicity associated with RXR agents is not known. Complement activation and secondary myocardial degeneration have been reported in pigs that received various forms of nanoparticles. A similar lesion was not present in pigs that received nanoparticles in this study, which indicates safety of the nanoparticles in a large animal model.

## ■ ASSOCIATED CONTENT

### ● Supporting Information

The Supporting Information is available free of charge on the ACS Publications website at DOI: 10.1021/acs.jmedchem.8b01387.

Method for selection of compounds for virtual screening, chemical characterization, mass and NMR spectra, histopathology results, and clinical pathology results from Oncopigs with different treatments (PDF)

Molecular formula string (CSV)

## ■ AUTHOR INFORMATION

### Corresponding Author

\*E-mail: dipanjan@illinois.edu.

### ORCID

Santosh K. Misra: 0000-0002-3313-4895

Dipanjan Pan: 0000-0003-0175-4704

### Author Contributions

◇M.Y., S.K.M., and A.K.D. contributed equally.

## Notes

The authors declare the following competing financial interest(s): Prof. Pan is the founder of three University start-ups; however, none of these entities supported this work.

## ■ ACKNOWLEDGMENTS

We thank Frederick Seitz Materials Research Laboratory for materials characterization techniques (DLS,  $\zeta$ -potential, TEM, and XRD), Noyes lab for NMR studies, Division of Animal Resources (DAR) for animal studies, and Veterinary medicine, UIUC, for histopathology facility. This project has been partially funded by University of Illinois and National Institutes of Health (Grant 1R42HL135965–01A1 (D. Pan)). We also extend our thanks to Children's Discovery Institute for financial assistance and American Heart Association via the Grant No. 18pre34080003/2018.

## ■ ABBREVIATION USED

RCM, rigid cored micelle; OCM, Oncopig cancer model; ANOVA, one-way analysis of variance; DOX, doxorubicin; AIM, ifosfamide; CTCL, cutaneous T cell lymphoma; RA, retinoic acid; calcd, calculated

## ■ REFERENCES

- (1) Matushansky, I.; Maki, R. G. Fighting Cancer through the Study of Sarcomas. *Am. Sci.* **2005**, *93*, 414–421.
- (2) Nathenson, M. J.; Sausville, E. Looking for Answers: the Current Status of Neoadjuvant Treatment in Localized Soft Tissue Sarcomas. *Cancer Chemother. Pharmacol.* **2016**, *78*, 895–919.
- (3) Tseng, W. W.; Somaiah, N.; Engleman, E. G. Potential for Immunotherapy in Soft Tissue Sarcoma. *Hum. Vaccines Immunother.* **2014**, *10*, 3117–3124.
- (4) Anderson, P. M.; Wiseman, G. A.; Erlandson, L.; Rodriguez, V.; Trotz, B.; Dubansky, S. A.; Albritton, K. Gemcitabine Radio-sensitization after High-Dose Samarium for Osteoblastic Osteosarcoma. *Clin. Cancer Res.* **2005**, *11*, 6895–6900.
- (5) Akatsuka, T.; Wada, T.; Kokai, Y.; Kawaguchi, S.; Isu, K.; Yamashiro, K.; Yamashita, T.; Sawada, N.; Yamawaki, S.; Ishii, S. Erbb2 Expression is Correlated with Increased Survival of Patients with Osteosarcoma. *Cancer* **2002**, *94*, 1397–1404.
- (6) Anderson, P. M.; Wiseman, G. A.; Dispenzieri, A.; Arndt, C. A.; Hartmann, L. C.; Smithson, W. A.; Mullan, B. P.; Bruland, O. S. High-Dose Samarium-153 Ethylene Diamine Tetramethylene Phosphonate: Low Toxicity of Skeletal Irradiation in Patients with Osteosarcoma and Bone Metastases. *J. Clin. Oncol.* **2002**, *20*, 189–196.
- (7) Burgert, E. O., Jr; Nesbit, M. E.; Garnsey, L. A.; Gehan, E. A.; Herrmann, J.; Vietti, T. J.; Cangir, A.; Tefft, M.; Evans, R.; Thomas, P. Multimodal Therapy for the Management of Nonpelvic, Localized Ewing's Sarcoma of Bone: Intergroup Study IESS-II. *J. Clin. Oncol.* **1990**, *8*, 1514–1524.
- (8) Ferrari, S.; Smeland, S.; Mercuri, M.; Bertoni, F.; Longhi, A.; Ruggieri, P.; Alvegard, T. A.; Picci, P.; Capanna, R.; Bernini, G.; et al. Neoadjuvant Chemotherapy with High-Dose Ifosfamide, High-Dose Methotrexate, Cisplatin, And Doxorubicin for Patients with Localized Osteosarcoma of the Extremity: A Joint Study by the Italian and Scandinavian Sarcoma Groups. *J. Clin. Oncol.* **2005**, *23*, 8845–8852.
- (9) Gorlick, R.; Huvos, A. G.; Heller, G.; Aledo, A.; Beardsley, G. P.; Healey, J. H.; Meyers, P. A. Expression of HER2/ErbB-2 Correlates with Survival in Osteosarcoma. *J. Clin. Oncol.* **1999**, *17*, 2781–2788.
- (10) Grier, H. E.; Krailo, M. D.; Tarbell, N. J.; Link, M. P.; Fryer, C. J.; Pritchard, D. J.; Gebhardt, M. C.; Dickman, P. S.; Perlman, E. J.; Meyers, P. A.; et al. Addition of Ifosfamide and Etoposide to Standard Chemotherapy for Ewing's Sarcoma and Primitive Neuroectodermal Tumor of Bone. *N. Engl. J. Med.* **2003**, *348*, 694–701.
- (11) Le Deley, M.-C.; Guinebretière, J.-M.; Gentet, J.-C.; Pacquement, H.; Pichon, F.; Marec-Bérard, P.; Entz-Werlé, N.;

Schmitt, C.; Brugières, L.; Vanel, D.; et al. SFOP OS94: A Randomised Trial Comparing Preoperative High-Dose Methotrexate Plus Doxorubicin to High-Dose Methotrexate Plus Etoposide and Ifosfamide in Osteosarcoma Patients. *Eur. J. Cancer* **2007**, *43*, 752–761.

(12) Susa, M.; Milane, L.; Amiji, M. M.; Hornicek, F. J.; Duan, Z. Nanoparticles: A Promising Modality in the Treatment of Sarcomas. *Pharm. Res.* **2011**, *28*, 260–272.

(13) Wagner, L. M.; Yin, H.; Eaves, D.; Currier, M.; Cripe, T. P. Preclinical Evaluation of Nanoparticle Albumin-Bound Paclitaxel for Treatment of Pediatric Bone Sarcoma. *Pediatric blood & cancer* **2014**, *61*, 2096–2098.

(14) Abe, S.; Seitoku, E.; Iwadera, N.; Hamba, Y.; Yamagata, S.; Akasaka, T.; Kusaka, T.; Inoue, S.; Yawaka, Y.; Iida, J.; et al. Estimation of Biocompatibility of Nano-Sized Ceramic Particles with Osteoblasts, Osteosarcomas and Hepatocytes by Static and Time-Lapse Observation. *J. Biomed. Nanotechnol.* **2016**, *12*, 472–480.

(15) Liu, Y.; Gunda, V.; Zhu, X.; Xu, X.; Wu, J.; Askhatova, D.; Farokhzad, O. C.; Parangi, S.; Shi, J. Theranostic Near-Infrared Fluorescent Nanoplatform for Imaging and Systemic SiRNA Delivery to Metastatic Anaplastic Thyroid Cancer. *Proc. Natl. Acad. Sci. U. S. A.* **2016**, *113*, 7750–7755.

(16) Makridis, A.; Tziomaki, M.; Topouridou, K.; Yavropoulou, M. P.; Yovos, J. G.; Kalogirou, O.; Samaras, T.; Angelakeris, M. A Novel Strategy Combining Magnetic Particle Hyperthermia Pulses with Enhanced Performance Binary Ferrite Carriers for Effective In Vitro Manipulation of Primary Human Osteogenic Sarcoma Cells. *Int. J. Hyperthermia* **2016**, *32*, 778–785.

(17) Zhang, B.-F.; Xing, L.; Qiao, J.-B.; Cui, P.-F.; Wang, F.-Z.; Zhang, J.-L.; Xu, C.-X.; Jiang, H.-L. In Vivo Synergistic Antitumor Effect and Safety of SiRNA and Lonidamine Dual-Loaded Hierarchical Targeted Nanoparticles. *Int. J. Pharm.* **2016**, *506*, 207–213.

(18) Reed, D. E.; Shokat, K. M. Targeting Osteosarcoma. *Proc. Natl. Acad. Sci. U. S. A.* **2014**, *111*, 18100.

(19) González-Fernández, Y.; Imbuluzqueta, E.; Patiño-García, A.; Blanco-Prieto, M. Antitumoral-Lipid-Based Nanoparticles: A Platform for Future Application in Osteosarcoma Therapy. *Curr. Pharm. Des.* **2015**, *21*, 6104–6124.

(20) Gu, X.; Ding, J.; Zhang, Z.; Li, Q.; Zhuang, X.; Chen, X. Polymeric Nanocarriers for Drug Delivery in Osteosarcoma Treatment. *Curr. Pharm. Des.* **2015**, *21*, 5187–5197.

(21) Akhtar, M. J.; Ahamed, M.; Alhadlaq, H. A.; Khan, M. M.; Alokayan, S. A. Glutathione Replenishing Potential of Ceo2 Nanoparticles in Human Breast and Fibrosarcoma Cells. *J. Colloid Interface Sci.* **2015**, *453*, 21–27.

(22) Duan, Z.; et al. Polymeric Nanoparticle-Based Delivery of MicroRNA-199a-3p Inhibits Proliferation and Growth of Osteosarcoma Cells. *Int. J. Nanomed.* **2015**, *10*, 2913–2924.

(23) Wang, B.; Yu, X.-C.; Xu, S.-F.; Xu, M. Paclitaxel and Etoposide Co-Loaded Polymeric Nanoparticles for the Effective Combination Therapy Against Human Osteosarcoma. *J. Nanobiotechnol.* **2015**, *13*, 22.

(24) Wójcik, M.; Lewandowski, W.; Król, M.; Pawłowski, K.; Mieczkowski, J.; Lechowski, R.; Zabiłska, K. Enhancing Anti-Tumor Efficacy of Doxorubicin by Non-Covalent Conjugation to Gold Nanoparticles - In Vitro Studies on Feline Fibrosarcoma Cell Lines. *PLoS One* **2015**, *10*, No. e0124955.

(25) Zabiłska-Koczywaś, K.; Wojtalewicz, A.; Lechowski, R. Current Knowledge on Feline Injection-Site Sarcoma Treatment. *Acta Vet. Scand.* **2017**, *59*, 47.

(26) Ni, M.; Xiong, M.; Zhang, X.; Cai, G.; Chen, H.; Zeng, Q.; Yu, Z. Poly(lactic-co-glycolic acid) Nanoparticles Conjugated with CD133 Aptamers for Targeted Salinomycin Delivery to CD133+ Osteosarcoma Cancer Stem Cells. *Int. J. Nanomed.* **2015**, *10*, 2537.

(27) Wang, Q.; Lv, L.; Ling, Z.; Wang, Y.; Liu, Y.; Li, L.; Liu, G.; Shen, L.; Yan, J.; Wang, Y. Long-Circulating Iodinated Albumin-Gadolinium Nanoparticles as Enhanced Magnetic Resonance and Computed Tomography Imaging Probes for Osteosarcoma Visualization. *Anal. Chem.* **2015**, *87*, 4299–4304.

(28) Bertrand, J.-R.; Pioche-Durieu, C.; Ayala, J.; Petit, T.; Girard, H. A.; Malvy, C. P.; Le Cam, E.; Treussart, F.; Arnault, J.-C. Plasma Hydrogenated Cationic Detonation Nanodiamonds Efficiently Deliver to Human Cells in Culture Functional SiRNA Targeting the Ewing Sarcoma Junction Oncogene. *Biomaterials* **2015**, *45*, 93–98.

(29) Altucci, L.; Gronemeyer, H. The Promise of Retinoids to Fight Against Cancer. *Nat. Rev. Cancer* **2001**, *1*, 181–193.

(30) Klopffer, J. P.; Sharma, V.; Berenz, A.; Hays, W. R.; Loi, M.; Pugazhenth, U.; Said, S.; Haugen, B. R. Retinoid and Thiazolidinedione Therapies in Melanoma: An Analysis of Differential Response Based on Nuclear Hormone Receptor Expression. *Mol. Cancer* **2009**, *8*, 16.

(31) Mohan, H. M.; Aherne, C. M.; Rogers, A. C.; Baird, A. W.; Winter, D. C.; Murphy, E. P. Molecular Pathways: The Role of NR4A Orphan Nuclear Receptors in Cancer. *Clin. Cancer Res.* **2012**, *18*, 3223–3228.

(32) Wagner, K. D.; Benchetrit, M.; Bianchini, L.; Michiels, J. F.; Wagner, N. Peroxisome Proliferator-Activated Receptor B/ $\Delta$  (Ppar $\beta$ / $\Delta$ ) is Highly Expressed in Liposarcoma and Promotes Migration and Proliferation. *Journal of pathology* **2011**, *224*, 575–588.

(33) Gallagher, R.; Keighley, J.; Tancabelic, J.; Garimella, R.; Pinson, D.; Templeton, K.; Tawfik, O. Clinicopathologic Correlation of Vitamin D Receptor Expression with Retinoid X Receptor and MIB-1 Expression in Primary and Metastatic Osteosarcoma. *Ann. Diagn. Pathol.* **2012**, *16*, 323–329.

(34) He, B.-C.; Chen, L.; Zuo, G.-W.; Zhang, W.; Bi, Y.; Huang, J.; Wang, Y.; Jiang, W.; Luo, Q.; Shi, Q.; et al. Synergistic Antitumor Effect of the Activated Ppargamma and Retinoid Receptors on Human Osteosarcoma. *Clin. Cancer Res.* **2010**, *16*, 2235–2245.

(35) Querfeld, C.; Nagelli, L. V.; Rosen, S. T.; Kuzel, T. M.; Guitart, J. Bexarotene in the Treatment of Cutaneous T-Cell Lymphoma. *Expert Opin. Pharmacother.* **2006**, *7*, 907–915.

(36) Cheng, C.; Michaels, J.; Scheinfeld, N. Alitretinoin: A Comprehensive Review. *Expert Opin. Invest. Drugs* **2008**, *17*, 437–443.

(37) Haydon, R. C.; Zhou, L.; Feng, T.; Breyer, B.; Cheng, H.; Jiang, W.; Ishikawa, A.; Peabody, T.; Montag, A.; Simon, M. A. Nuclear Receptor Agonists as Potential Differentiation Therapy Agents for Human Osteosarcoma. *Clin. Cancer Res.* **2002**, *8*, 1288–1294.

(38) Nagpal, S.; Cai, J.; Zheng, T.; Patel, S.; Masood, R.; Lin, G. Y.; Friant, S.; Johnson, A.; Smith, D. L.; Chandraratna, R.; Gill, P. S. Retinoid Antagonism of NF-IL6: Insight into the Mechanism of Antiproliferative Effects of Retinoids in Kaposi's Sarcoma. *Mol. Cell. Biol.* **1997**, *17*, 4159–4168.

(39) Tontonoz, P.; Singer, S.; Forman, B. M.; Sarraf, P.; Fletcher, J. A.; Fletcher, C. D.; Brun, R. P.; Mueller, E.; Altiock, S.; Oppenheim, H. Terminal Differentiation of Human Liposarcoma Cells Induced by Ligands for Peroxisome Proliferator-Activated Receptor Gamma and the Retinoid X Receptor. *Proc. Natl. Acad. Sci. U. S. A.* **1997**, *94*, 237–241.

(40) Salbert, G.; Fanjul, A.; Piedrafita, F. J.; Lu, X. P.; Kim, S.-J.; Tran, P.; Pfahl, M. Retinoic Acid Receptors and Retinoid X Receptor-Alpha Down-Regulate the Transforming Growth Factor-Beta 1 Promoter by Antagonizing AP-1 Activity. *Mol. Endocrinol.* **1993**, *7*, 1347–1356.

(41) Schook, L. B.; Rund, L.; Begnini, K. R.; Remião, M. H.; Seixas, F. K.; Collares, T. Emerging Technologies to Create Inducible and Genetically Defined Porcine Cancer Models. *Front. Genet.* **2016**, *7*, 28.

(42) Schachtschneider, K. M.; Madsen, O.; Park, C.; Rund, L. A.; Groenen, M. A.; Schook, L. B. Adult Porcine Genome-Wide DNA Methylation Patterns Support Pigs as a Biomedical Model. *BMC Genomics* **2015**, *16*, 743.

(43) Schook, L. B.; Collares, T. V.; Hu, W.; Liang, Y.; Rodrigues, F. M.; Rund, L. A.; Schachtschneider, K. M.; Seixas, F. K.; Singh, K.; Wells, K. D.; et al. A Genetic Porcine Model of Cancer. *PLoS One* **2015**, *10*, No. e0128864.

(44) Misra, S. K.; Ye, M.; Kim, S.; Pan, D. Defined Nanoscale Chemistry Influences Delivery of Peptidotoxins for Cancer Therapy. *PLoS One* **2015**, *10*, No. e0125908.

- (45) Misra, S. K.; Jensen, T. W.; Pan, D. Enriched Inhibition of Cancer and Stem-Like Cancer Cells via STAT-3 Modulating Niclocelles. *Nanoscale* **2015**, *7*, 7127.
- (46) Misra, S. K.; Kus, J.; Kim, S.; Pan, D. Nanoscopic Poly-DNA-Cleaver for Breast Cancer Regression with Induced Oxidative Damage. *Mol. Pharmaceutics* **2014**, *11*, 4218.
- (47) Misra, S. K.; Ye, M.; Kim, S.; Pan, D. Highly Efficient Anti-Cancer Therapy Using Scorpion 'NanoVenin'. *Chem. Commun.* **2014**, *50*, 13220.
- (48) Misra, S. K.; Ghoshal, G.; Gartia, M. R.; Wu, Z.; De, A. K.; Ye, M.; Bromfield, C. R.; Williams, E. M.; Singh, K.; Tangella, K. V.; et al. Trimodal Therapy: Combining Hyperthermia with Repurposed Bexarotene and Ultrasound for Treating Liver Cancer. *ACS Nano* **2015**, *9*, 10695.
- (49) Szebeni, J.; Bedőcs, P.; Rozsnyay, Z.; Weiszár, Z.; Urbanics, R.; Rosivall, L.; Cohen, R.; Garbuzenko, O.; Báthori, G.; Tóth, M.; et al. Liposome-Induced Complement Activation and Related Cardiopulmonary Distress in Pigs: Factors Promoting Reactogenicity of Doxil and Ambisome. *Nanomedicine* **2012**, *8*, 176–184.
- (50) Edwardson, D.; Narendrula, R.; Chewchuk, S.; Mispel-Beyer, K.; Mapletoft, J.; Parissenti, M. Role of Drug Metabolism in the Cytotoxicity and Clinical Efficacy of Anthracyclines. *Curr. Drug Metab.* **2015**, *16*, 412–426.
- (51) Gomez-Lechon, M. J.; Castell, J. V.; Donato, M. T. Hepatocytes—The Choice to Investigate Drug Metabolism and Toxicity in Man: In Vitro Variability as a Reflection of In Vivo. *Chem.-Biol. Interact.* **2007**, *168*, 30–50.
- (52) Szotáková, B.; Baliharová, V.; Lamka, J.; Nožinová, E.; Wsól, V.; Velí, J.; Machala, M.; Neča, J.; Souček, P.; Šusová, S. Comparison of In Vitro Activities of Biotransformation Enzymes in Pig, Cattle, Goat and Sheep. *Res. Vet. Sci.* **2004**, *76*, 43–51.
- (53) Achour, B.; Barber, J.; Rostami-Hodjegan, A. Cytochrome P450 Pig Liver Pie: Determination of Individual Cytochrome P450 Isoform Contents in Microsomes from Two Pig Livers Using Liquid Chromatography in Conjunction with Mass Spectrometry. *Drug Metab. Dispos.* **2011**, *39*, 2130–2134.
- (54) Werck-Reichhart, D.; Feyereisen, R. Cytochromes P450: A Success Story. *Genome biology* **2000**, *1*, reviews3003.1.
- (55) Ortiz de Montellano, P. R.; De Voss, J. J. Oxidizing Species in the Mechanism of Cytochrome P450. *Nat. Prod. Rep.* **2002**, *19*, 477–493.
- (56) Ashla, A. A.; Hoshikawa, Y.; Tsuchiya, H.; Hashiguchi, K.; Enjoji, M.; Nakamuta, M.; Taketomi, A.; Maehara, Y.; Shomori, K.; Kurimasa, A.; et al. Genetic Analysis of Expression Profile Involved in Retinoid Metabolism in Non-Alcoholic Fatty Liver Disease. *Hepatol. Res.* **2010**, *40*, 594–604.
- (57) Pan, C. J.; Hoepfner, W.; Chou, J. Y. Induction of Phosphoenolpyruvate Carboxykinase Gene Expression by Retinoic Acid in an Adult Rat Hepatocyte Line. *Biochemistry* **1990**, *29*, 10883–10888.
- (58) Kalaany, N. Y.; Mangelsdorf, D. J. LXRS and FXR: The Yin And Yang of Cholesterol and Fat Metabolism. *Annu. Rev. Physiol.* **2006**, *68*, 159–191.
- (59) Desvergne, B.; Wahli, W. Peroxisome Proliferator-Activated Receptors: Nuclear Control of Metabolism. *Endocr. Rev.* **1999**, *20*, 649–688.
- (60) Lucas, P. C.; O'Brien, R. M.; Mitchell, J. A.; Davis, C. M.; Imai, E.; Forman, B. M.; Samuels, H. H.; Granner, D. K. A Retinoic Acid Response Element is Part of a Pleiotropic Domain in the Phosphoenolpyruvate Carboxykinase Gene. *Proc. Natl. Acad. Sci. U. S. A.* **1991**, *88*, 2184–2188.
- (61) Hall, R. K.; Scott, D. K.; Noisin, E. L.; Lucas, P. C.; Granner, D. K. Activation of the Phosphoenolpyruvate Carboxykinase Gene Retinoic Acid Response Element is Dependent on a Retinoic Acid Receptor/ Coregulator Complex. *Mol. Cell. Biol.* **1992**, *12*, 5527–5535.
- (62) Shin, D.-J.; Tao, A.; McGrane, M. M. Effects of Vitamin A Deficiency and Retinoic Acid Treatment on Expression of a Phosphoenolpyruvate Carboxykinase-Bovine Growth Hormone Gene in Transgenic Mice. *Biochem. Biophys. Res. Commun.* **1995**, *213*, 706–714.
- (63) Wolchok, J. D.; Kluger, H.; Callahan, M. K.; Postow, M. A.; Rizvi, N. A.; Lesokhin, A. M.; Segal, N. H.; Ariyan, C. E.; Gordon, R.-A.; Reed, K.; et al. Nivolumab Plus Ipilimumab in Advanced Melanoma. *N. Engl. J. Med.* **2013**, *369*, 122–133.
- (64) Topalian, S. L.; Sznol, M.; McDermott, D. F.; Kluger, H. M.; Carvajal, R. D.; Sharfman, W. H.; Brahmer, J. R.; Lawrence, D. P.; Atkins, M. B.; Powderly, J. D.; et al. Survival, Durable Tumor Remission, and Long-Term Safety in Patients with Advanced Melanoma Receiving Nivolumab. *J. Clin. Oncol.* **2014**, *32*, 1020–1030.
- (65) Schachtschneider, K. M.; Liu, Y.; Mäkeläinen, S.; Madsen, O.; Rund, L. A.; Groenen, M. A.; Schook, L. B. Oncopig Soft-Tissue Sarcomas Recapitulate Key Transcriptional Features of Human Sarcomas. *Sci. Rep.* **2017**, *7*, 2624.
- (66) Ian, F. R. *Culture of Animal Cells: A Manual of Basic Technique and Specialized Applications*; Wiley-Sons: New York, 2010.
- (67) van Meerloo, J.; Kaspers, G. J.; Cloos, J. Cell Sensitivity Assays: The MTT Assay. *Methods Mol. Biol.* **2011**, *731*, 237–245.